Electronic Supplementary Material (ESI) for Dalton Transactions.

Supporting Information

Direct solvothermal preparation of nanostructured fluoride aerogels based on AlF_3

Aleš Štefančič, Darinka Primc, Gašper Tavčar, Tomaž Skapin*

*E-mail address: tomaz.skapin@ijs.si

1) Chemicals and experimental procedures

Caution. *The work includes the use of anhydrous hydrogen fluoride, aHF, that is highly toxic and potentially dangerous. It must be handled with high precaution by using appropriate apparatus and protective clothing.*

1.1 Chemicals.

Aluminum isopropoxide, $Al(O^iPr)_3$, and all organic solvents used within this study (listed in Tables 1 and S2) were analytical grade chemicals (Merck). Anhydrous hydrogen fluoride (aHF; min. 99.9 %, Fluka) was used as a fluorinating agent in the preparation of fluoride sol/gel precursors. 1,1,2-Trichloro-1,2,2-trifluoroethane (CCl_2FCClF_2, CFC-113; 99 %, Aldrich) was used in catalytic isomerization tests. In some experiments, dichlorodifluoromethane (CCl_2F_2, CFC-12; 99,9 %, ICI) was employed as a post-treatment reagent for the reduction of residual methoxy species. All the chemicals mentioned above were used as received.

1.2 Experimental procedures.

1.2.1 Preparation of fluoride precursors. In general, fluoride precursors in the form of sols or gels were prepared according to the fluoride sol-gel procedure[1,2]. In our preparations, the original procedure[1,2] was slightly modified, *i.e.* instead of adding HF pre-dissolved in alcohol or ether, gaseous aHF was dosed directly into the reaction vessel containing a solution of $Al(O^iPr)_3$ in the organic solvent. In this way, a separate step of HF-solution preparation is eliminated, and a better control over the HF-dosing is achieved. In addition, all operations with the potentially harmful HF are carried out in a closed system that prevents contact with ambient atmosphere, and improves safety. Wet fluoride precursors were prepared on a vacuum line constructed entirely of HF-resistant materials, *i.e.* nickel, and fluoropolymers, *e.g.* polytetrafluoroethylene (PTFE) or the transparent copolymer of hexafluoropropylene and tetrafluoroethylene (FEP).

Typical preparation run:. In a typical run, 10 g of $Al(O^iPr)_3$ were weighed in a dry-box into a 500 cm^3 FEP reaction vessel equipped with a magnetic stirrer, and 110±10 cm^3 of the organic solvent were added in air; the resulting concentrations of $Al(O^iPr)_3$ were in the range of 0.4–0.5 mol L^{-1}. The solvents used in this stage are hereafter denoted as primary solvents. The reaction vessel was connected to a vacuum line and stirred for two hours to obtain homogeneous solutions/suspensions of $Al(O^iPr)_3$. To prevent overheating due to the exothermic reaction with HF, the reaction vessel was immersed in a water bath kept at room temperature. During vigorous mixing, a stoichiometric amount (according to Eq. 1) of gaseous aHF was dosed into the reaction vessel within one hour. The required amount of aHF was dosed from a pre-weighed and calibrated container filled with liquid aHF. Container was made from a 6 mm ID FEP tube. After HF addition, intensive mixing was continued for 30 minutes to assure homogeneity. The products were then aged in a closed vessel overnight, for approximately 16 hours.

$$Al(O^iPr)_3 + 3HF \rightarrow AlF_3 + 3^iPrOH \quad (1)$$

1.2.2 Drying at sub- or supercritical conditions. Aged wet fluoride precursors described above were dried in an autoclave at sub- or supercritical conditions with respect to the organic solvent used. Critical properties of the applied solvents are presented in Table S1. Drying procedure was very similar to that used in the preparation of Al_2O_3-based aerogels[3,4], only the key aspects of the current procedure are therefore outlined. Wet precursors were transferred into a 530 cm^3 glass liner of the 1-litre autoclave. Solvents used in this stage, further on denoted as additional solvents, were used for rinsing the FEP vessel and for filling both the glass liner and the autoclave. After closure, autoclave was pressurized to 8 MPa with dry nitrogen and linearly heated to the final temperature within 2–3 hours; autoclave was then kept at

the final temperature during stabilization (0–1 hour), depressurization (1-2-3 hours), and evacuation/N_2-flushing cycles (approximately 2 hours). Underlined values are the times used in majority of the drying runs reported here (standard drying program). As found earlier[3,5,6] and confirmed also in this study (see Figure S1), in the presence of acidic solids, and under solvothermal conditions encountered during the supercritical drying, alcohols are readily dehydrated to ethers. Accordingly, final water contents in the released condensates, determined in some runs, were in the range of 1.5–4.3 wt.%. Since the critical conditions of the mixed liquid phases may be strongly altered by the water formed in-situ, majority of supercritical drying runs were performed at 300 °C, *i.e.* well above the critical temperatures of the pure organic solvents employed (see Table S1). To investigate the effect of temperature, some runs were performed at lower temperature (260 °C) which was still for 20–25 °C above the critical temperatures of the solvents. Pressure in the autoclave was regulated manually. Maximum pressure was maintained at 15±1 MPa by releasing the vapors through a venting valve. Illustrative course of a supercritical drying run is shown in Figure S1. After depressurization and flushing with N_2, autoclave was cooled overnight. Solid products were recovered in air.

For comparison, one drying run was carried out at subcritical conditions, at 200 °C. Product from this run was a typical compact xerogel with a strongly contracted structure. Various types of products, *i.e.* aerogels, collapsed powdery products and a xerogel, marked as A#, C# and X#, respectively, have been prepared within this work. Main preparation conditions and some properties of the products are summarized in Table 1 for the most representative materials, and in Table S2 for some additional illustrative products.

1.2.3 Post-treatment of solid products. To determine the thermal behavior of residual species, portions of some products were subjected to additional drying in dynamic vacuum at 300 °C for several hours. These products are marked with the extension -D (Table 1). Classical route to HS-AlF_3 includes a so-called activation step, i.e. treatment with a mild fluorinating agent at moderate temperatures, like CCl_2F_2 at 300 °C, to remove the residual organic species and surface OH groups that presumably block the surface Lewis acid sites.[1,2,6,7] In order to verify the chemical stability of surface methoxy species, one aerogel was therefore treated at 300 °C for 1 hour in a flow of CCl_2F_2 (20 vol.%) diluted with nitrogen. This sample is marked with the extension -F (Table 1).

Table S1. Critical constants for the solvents applied in the current study (data extracted from CRC Handbook of Chemistry and Physics, 84th ed., CRC Press, 2003).

Solvent	Critical temperature, T_c (°C)	Critical pressure, P_c (MPa)
MeOH	239.4	8.08
EtOH	240.9	6.14
^{i}PrOH	235.2	4.76
^{i}BuOH	274.7	4.30
EtOAc	250.2	3.87
Et_2O	193.6	3.64
n-hexane	234.5	3.03
H_2O	374.0	22.06

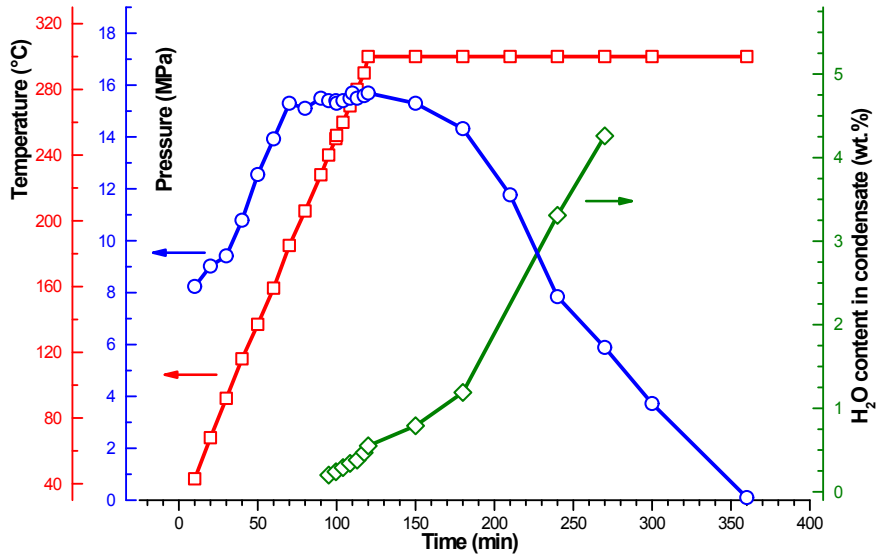

Figure S1. Course of supercritical drying of product A6; figure shows the time-profiles for temperature (□), pressure (○), and H_2O-content in the released condensate (◊). In this specific case a modified drying program was used (heating: 2 h, stabilization: 0 h, depressurization: 4 h); majority of drying runs was performed using a standard program (heating: 3 h, stabilization: 1 h, depressurization: 2 h). Note: H_2O is formed in-situ as a result of the dehydration of alcohols to ethers; reaction is catalyzed by the formed solid phase that acts as an acid catalyst.

2) Additional materials

Table S2 complements Table 1 and summarizes the key preparation conditions and properties of some additional relevant products prepared within this study. Strong effect of primary/additional solvents is demonstrated; very voluminous aerogels with specific surface areas that in most cases exceed 100 m^2 g^{-1} are obtained only in runs where ^{i}PrOH is used as a primary and MeOH as an additional solvent.

Table S2. Preparation conditions and some properties of additional representative materials obtained by supercritical drying

Sample[a]	Solvent[b]	Temp. (°C)	Note	N_2-physisorption			Chemical analysis (wt. %)					F/Al ratio
				BET area (m^2 g^{-1})	Pore volume (ads.) (cm^3 g^{-1})	Av. pore diam. (ads.) (nm)	Al	F	C	H	Mass differ-rence[c]	
A4	EtOH / MeOH	300		43	0.09	8.9	30.2	62.75			7.1	2.95
A5	EtOAc / MeOH	300		55	0.12	8.6	27.7	63.05			7.3	3.02
A6	^{i}PrOH / MeOH	300	rapid heating (2 h), slow release (4 h)	78	0.14	7.1	30.1	60.8			9.1	2.87
A7	^{i}PrOH / MeOH	260	rapid heating (2 h), quick release (1 h)	126	0.25	7.8	28.8	59.4			11.8	2.93
C2	Et_2O / MeOH	300		82	0.21	10.1	29.55	61.55			8.9	2.96
C3	n-hexane / MeOH	300		72	0.16	8.8	29.75	61.7			8.6	2.95
C4	^{i}BuOH / MeOH	300		61	0.14	9.1	29.8	59.8			10.4	2.85
C5	^{i}PrOH / ^{i}PrOH	300		42	0.13	12.7	30.3	62.2	<0.3[d]	0.71	7.5	2.92
C6	^{i}PrOH / Et_2O	300		28	0.10	14.6	30.55	61.4			8.1	2.85

[a]A-aerogel, C-collapsed material; [b]primary/additional solvent(s) used; [c]Mass difference (MD) defined as: MD = (100 – ∑wt. % (F + Al)); [d]Below the detection limit.

3) Supplementary IR spectra and possible assignments

3.1 Spectra of additional products

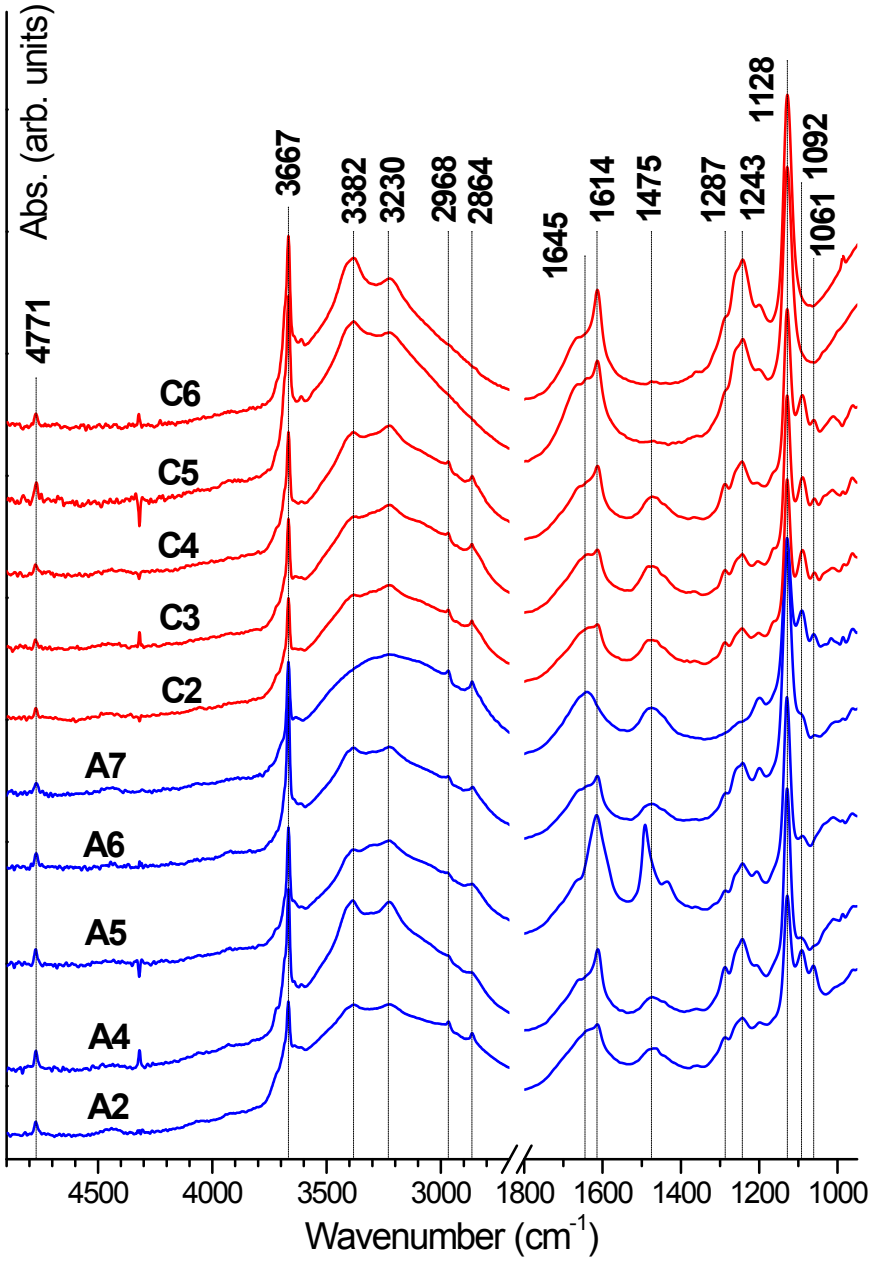

Figure S2. Normalized IR absorption spectra of some additional products in the form of aerogels (A - blue tracks) or collapsed products (C – red tracks); properties of these products are given in Table 1 for sample A2, and in Table S2 for all other samples. Only the most indicative spectral ranges, 4900–2700 and 1800–950 cm^{-1}, are shown. For the assignation of the indicated bands see Table S3.

3.2 Interpretation of spectra with possible assignments

All spectra show a broad and intense absorption band in the range of 800–550 cm^{-1} with the maximum at about 660–650 cm^{-1}, attributed to the ν(Al–F) and δ(Al–F) vibrations of AlF_3[8] (for clarity, this region is not shown in the spectra presented here and in the article).

3.2.1 OH/H_2O species

In the IR spectra of all materials dried at supercritical conditions (Figures 2 and S2), intense and relatively sharp bands at 4771, 3667, and 1128 cm^{-1} are observed, while in that for sample X1 only the band at 3667 cm^{-1} with a much lower intensity can be noticed. According to previous studies of a $AlF_{3-x}(OH)_x \cdot yH_2O$ series of compounds[9–11], these very characteristic bands can be ascribed to ν+δ(O–H), ν(O–H), and δ(O–H) vibrations (Table S3), respectively, of isolated bridged OH groups that replace some of the F^- ions in the HTB-AlF_3 and related crystal structures. Isolated bridged OH groups are therefore characteristic for ordered crystalline structures what explains an almost complete absence of these entities in poorly crystalline X1.

Common features of all spectra are the broad bands in the 3700–2700 and 1720–1560 cm^{-1} regions (Figures 2 and S2) which can be ascribed to the ν(H–O–H) and δ(H–O–H) vibrational modes of molecular H_2O[9,11,12] (Table S3), respectively. Molecular H_2O can be present either as crystal (structural) H_2O or as adsorbed H_2O[11]. In addition to the broad background bands, distinctive additional bands at 3382, 3230, 1614, 1287, and 1243 cm^{-1} are visible for the products obtained at 300 °C, and with a lesser intensity for those obtained at 260 °C. These spectral features are however not present in the spectrum of the xerogel, X1, that was prepared at 200 °C. According to XRD measurements, observed trend could lead to the conclusion that these bands could correspond to structural H_2O species in crystalline hydrated phases that are formed at higher temperatures. However, all these bands disappear after additional evacuation at 300 °C leaving only the two broad features at about 3250, and 1640 cm^{-1} (Figure 3). This indicates that the related H_2O species are relatively weakly bonded and can be therefore ascribed to adsorbed forms of H_2O. The apparent contradiction, *i.e.* higher amounts of adsorbed H_2O found at higher temperatures, can be explained by the increased dehydration of alcohols at higher temperatures[13,14] that results in higher levels of H_2O in the liquid phase what may, in turn, lead to enhanced hydration and hydrolysis. Namely, in a previous study of aluminum hydroxyfluorides with pyrochlore structure, two δ(H–O–H) modes in the range of 1650–1600 cm^{-1} were related to H_2O species engaged in different hydrogen-bonded configurations that depend on the specific anionic environments; *i.e.* a band at 1645 cm^{-1} was assigned to an H-donor-type of interaction with the surface fluoride, Al–F···H–OH (I); while that at 1605 cm^{-1} was assigned to an H-acceptor-type of interaction with acidic OH groups, Al–O–H···OH_2 (II).[15] Moreover, bands observed at 1255 and 1200 cm^{-1} were assigned to perturbed Al–OH groups, *e.g.* like those in configuration II.[15] It should be also noted that spectra, very similar to those reported here, were reported for HS-β-$AlF_{3-x}(OH)_x$.[9] In these spectra, an unassigned band at about 1240 cm^{-1} can be noticed that disappears after heating at 300 °C. According to these precedents, it is reasonable to assign the bands at 1287 and 1243 cm^{-1} to the δ(O–H) modes of perturbed OH groups[11,15], and the band at 1614 cm^{-1} to the δ(H–O–H) mode of H_2O hydrogen bonded to these perturbed OH groups (configuration II). The latter species very likely originate from hydrolysis processes that become more pronounced at higher temperatures.

In addition to the relatively labile adsorbed H_2O, a considerable amount of H_2O is strongly retained by the solids even after prolonged evacuation at 300 °C, as evidenced by the persistence of the two broad bands at about 3250, and 1645 cm^{-1} in the spectra of all products (Figures 2, 3 and S2). Similar thermal behavior was observed for HS-β-$AlF_{3-x}(OH)_x$.[9] Related H_2O species exhibit a high thermal and chemical stability and are not affected to a greater extent by the employed post-treatment procedures (Figure 3). It

can be assumed that these H_2O species are located in the bulk solid phase, most likely within the channels of the HTB-AlF_3 structure, and can therefore be regarded as bulk H_2O. As clearly demonstrated in previous studies[16,17], channels in related AlF_3 structures with diameters of 0.242–0.330 nm can accommodate only small molecular entities, like H_2O. Owing to the strong hydrogen bonding, movability of H_2O molecules confined within the channels is considerably reduced which results in a strong retention and, consequently, in a very slow release of H_2O from such materials.[16,17] Earlier it was also proposed that H_2O removal leads to some hydration and hydroxylation that may result in a partial hydrolysis of the surface.[17] According to the current IR investigations, the latter processes take place prevalently during the solvothermal preparation and are apparently less important in the post-treatment procedures used here. Adsorbed H_2O and surface OH groups are efficiently removed by evacuation at 300 °C (*cf.* the as-prepared and additionally dried, -D, samples in Figure 3). Thermally more stable species, *i.e.* strongly retained bulk H_2O and isolated OH groups, reside in the channels of the HTB structure. However, both the absence of perturbed OH groups and the location of the δ(H–O–H) mode at 1640 cm^{-1} in products treated at 300 °C indicate that there is no appreciable interaction between the two species. This may suggest that within the HTB channels H_2O is prevalently hydrogen bonded to fluoride sites (configuration I) and is not interfering with isolated OH groups.

3.2.2 Methoxy (MeO) species

IR spectra of some products show supplementary bands that can be assigned to residual organic species. Presence of these species in MeOH-derived products was confirmed by chemical analysis (Tables 1 and S2). Although the determined C-contents are relatively low, considering the applied solvothermal conditions and relatively large amounts of organic solvents used in the preparation, IR spectra (Figures 2, 3 and S2) show distinctive bands at 2968, 2864, 1475, 1092, and 1061 cm^{-1}. Based on previous reports on the interaction of MeOH[18,19] or MeCl[20] with Al_2O_3, these bands are assigned, respectively, to $\nu_{as}(CH_3)$, $\nu_s(CH_3)$, $\delta_{s+as}(CH_3)$, rocking(CH_3), and ν(C–O) modes of the methoxy (MeO) species linked to surface aluminum sites, Al–OMe, (Table S3). However, most indicative are the $\nu(CH_3)$ and $\delta(CH_3)$ modes located at 2968, 2864, and 1475 cm^{-1}; identification and assignment of bands in the range of 1200–1000 cm^{-1} is more ambiguous because of the possible overlapping with various δ(O–H) modes mentioned above.

It is important to note that in the current products only organic residues related to the MeOH-derived MeO species can be perceived. All other organic solvents used within this study apparently do not form stable organic residues at detectable levels, *e.g.* in the two products prepared without using MeOH, C1 and C5, amounts of residual organic species were below the measurable levels, as indicated by chemical analysis and IR spectroscopy. For the ^{i}PrOH-derived C5 (Figure S2 and Table S2), that is a direct analogue of the dry-gel intermediates in the preparation of HS-AlF_3[1,2], the complete lack of any C-containing residues clearly demonstrates that in the current preparations the conversion of $Al(O^iPr)_3$ to fluoride is practically quantitative and that the ^{i}PrO species, if retained or formed, are not stable under the applied solvothermal conditions and therefore do not remain in the solid product.

Table S3. Possible assignments of the relevant absorption bands in the IR spectra of the as-prepared fluoride materials investigated within this study (corresponding spectra are shown in Figure S2, and in Figures 2 and 3 in the paper)

Vibrational Frequency (cm^{-1})	**Mode Assignment**	**Possible Species**	**Ref.**
Weakly bonded (labile) species[a]			
3382	ν(H–O–H)	molecular H_2O (adsorbed)	9–12, 15
3230	ν(H–O–H)		
1614	δ(H–O–H) (e.g. in H-acceptor-type interaction, Al–O–H···OH_2)[15]		
1243 1287	δ(O–H)	perturbed (distorted) bridged Al–OH	11, 15
Strongly bonded (stable) species[b]			
~3250 (very broad)	ν(H–O–H)	molecular H_2O (bulk)	9, 11, 12, 15
~1645 (broad)	δ(H–O–H) (e.g. in H-donor-type interaction, Al–F···H–OH)[15]		
2968	$\nu_{as}(CH_3)$	methoxide, Al–OCH_3	18–20
2864	$\nu_{s}(CH_3)$		
~1475 (1500–1420; several overlapping bands)	$\delta_{s+as}(CH_3)$		
1092	rocking(CH_3) (?)		
1061	ν(C–O)		
4771	ν+δ(O–H)	isolated bridged Al–OH (preferentially located within the channels of the HTB structure)	9–11, 16
3667	ν(O–H)		
1128	δ(O–H)		

[a]Species removed by additional drying in vacuum at 300 °C (Figure 3 in the article); [b]Species that are not affected to a greater extent by additional drying at 300 °C (Figure 3 in the article)

4) Comparison of different batches of products

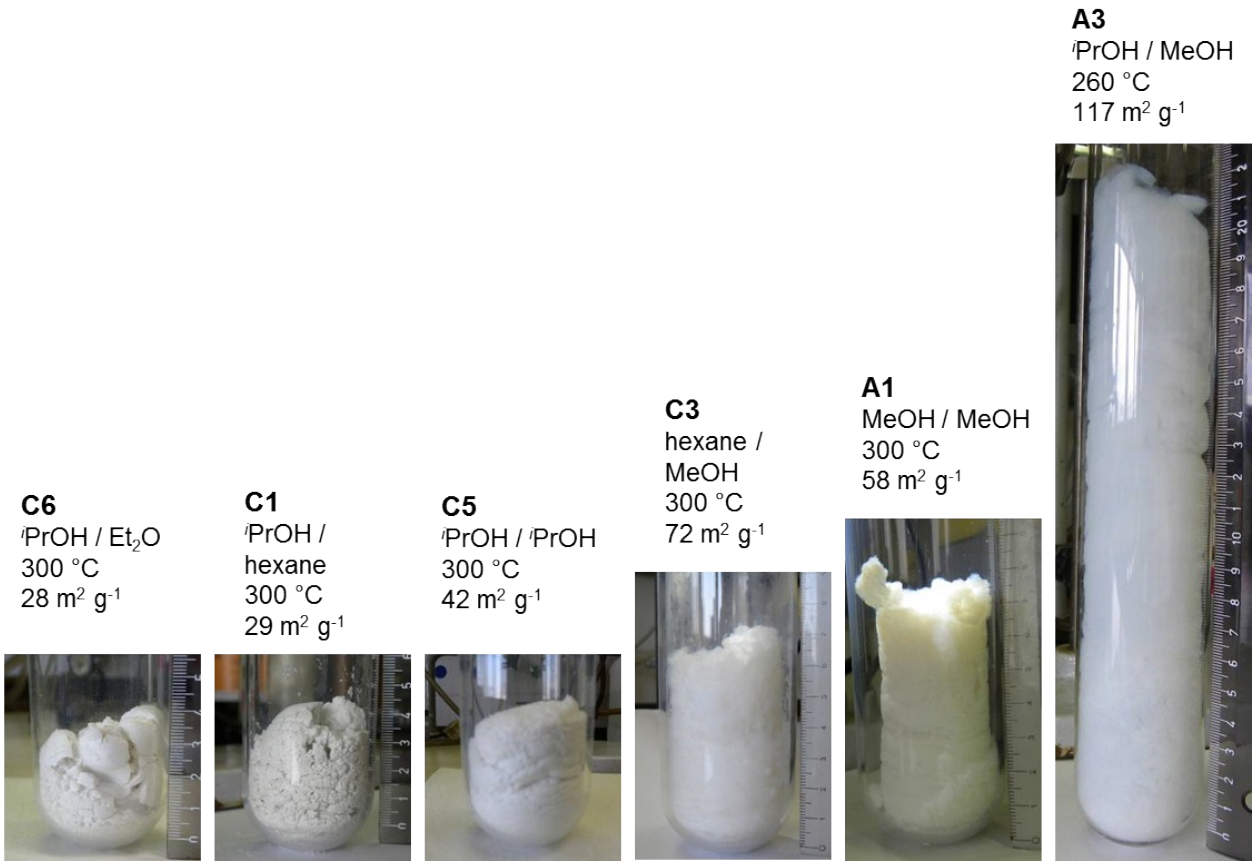

Figure S3. Visual comparison of products obtained by supercritical drying of identical batches of various fluoride precursors is given. Left: typical strongly collapsed (powdery) products (C1, C5 and C6); middle: collapsed product (C3); right: typical voluminous (aerogel-like) products (A1 and A3). For each product, primary/additional solvents, drying temperature, and BET surface area are given. Volume of the most expanded product (A3) is more than five-times larger than that of strongly collapsed products. Photos are approximately to scale.

5) Additional TEM analyses

5.1 Aerogel A3

TEM analysis of aerogel A3 (Figures S4a and S4b) reveals the presence of uniform elongated nanoparticles, i. e. nanorods with lengths of 100–150 nm and diameter of 5–20 nm. Size and morphology of the nanoparticles are not affected to a greater extent by additional thermal treatment at 300 °C (cf. Figures S4a and S4b). Detailed HRTEM examination (Figure S4c) reveals that the nanorods consist of smaller crystalline nanoparticles uniformly embedded in the middle of the larger amorphous matrix nanorods. Typically, these crystalline areas are elongated along the longer dimension of the matrix nanorods. The measured distance between lattice fringes of approximately 0.35 nm corresponds to the distance between {110} and {002} planes of the hexagonal β-AlF_3.

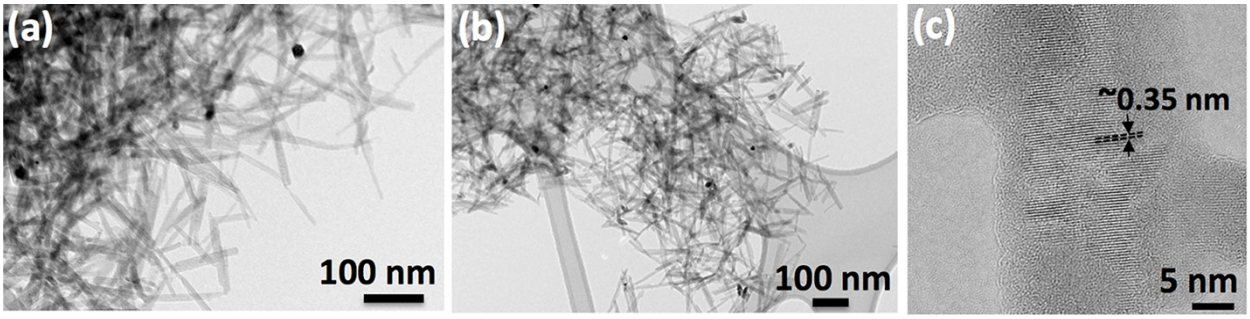

Figure S4. Representative TEM images of typical nanorods in aerogel A3: (a) as-prepared, (b) after prolonged thermal treatment at 300 °C in vacuum; (c) HRTEM image of a single hexagonal nanorod showing crystalline areas embedded in an amorphous matrix.

5.2 Xerogel X1

TEM analysis of xerogel X1 obtained by solvothermal treatment at 200 °C (Figure S5a) reveals the presence of irregularly shaped elongated nanoparticles of rather poor crystalline order. Detailed HRTEM analysis (Figure S5b) reveals the presence of small crystalline areas of approximately 3–5 nm, relatively randomly distributed within the amorphous matrix of the nanorods. The measured distances between lattice fringes of around 0.35 nm and 0.23 nm correspond to the distances between {110} and {202} planes of β- AlF_3, respectively.

Morphological characteristics and surface area of this product resemble very much those of the HS-AlF_3 obtained by the oxidative decomposition of hydrazinium fluoroaluminate in aHF.[21] Although these HS-AlF_3 products were amorphous to X-rays, 3 nm crystallites of α- and β-AlF_3 embedded in an amorphous phase could be identified by TEM. Current xerogel X1 exemplifies therefore the initial stage of ordering, crystallization, and particle growth.

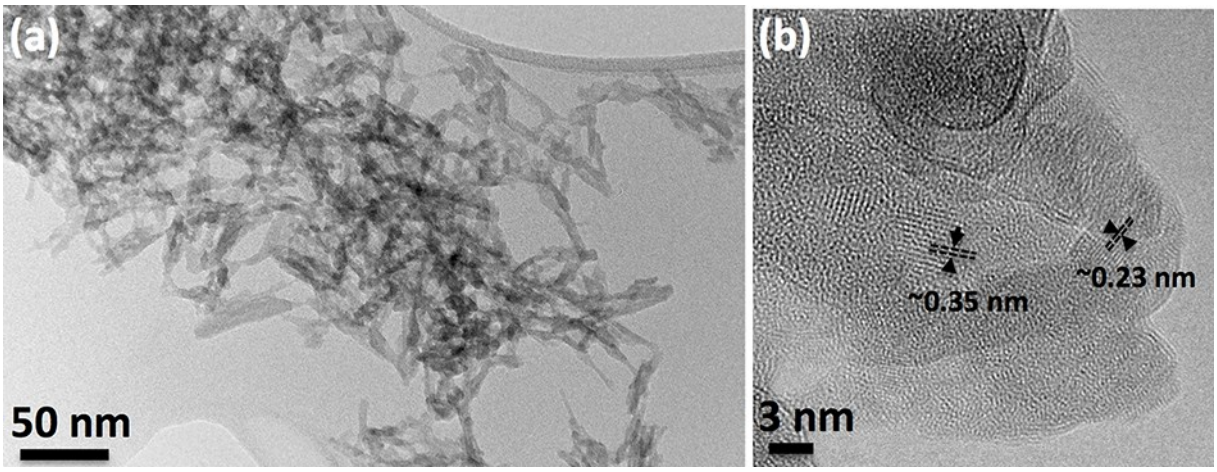

Figure S5. Representative TEM images of xerogel X1: (a) irregular nanorods; (b) HRTEM image shows small crystalline areas randomly distributed within the amorphous matrix.

6) Catalytic behavior

Test catalytic reaction: For some representative products, catalytic behaviour towards isomerization of CCl_2FCClF_2 was examined under steady flow conditions. Experimental setup and reaction conditions were the same as in previous studies[4,21,22] which allows a direct comparison with diverse Lewis acidic catalysts based on AlF_3. Materials used in catalytic tests are marked with the extension -C (Table 1 in the article).

Results: A series of catalytic tests was performed to gain some additional insights into the surface characteristics of representative products. Isomerization of CCl_2FCClF_2 was used as a test catalytic reaction since it allows direct comparisons with well-defined AlF_3-based catalyst examined in earlier studies.[4,21] There is a consensus[6,23,24] that activity in this isomerization reaction demonstrates the presence of relatively strong Lewis acidity. Data of isomerization tests are summarized in Table S4, where only the yields of unconverted starting substance, CCl_2FCClF_2, and of the key isomerization product, CCl_3CF_3, are given. To ease the comparison, some reference data from a previous study of diverse AlF_3-based materials[21] are also included. In all cases, materials were firstly activated in a flow of CCl_2FCClF_2 at up to 350 °C and were then tested at 300 °C.

Both aerogels, A1 and A3, show very low catalytic activity at 300 °C, similar to that of the reference β-AlF_3. One could presume that similar catalytic behaviour arises from the structural similarity of these materials. However, for β-AlF_3, a clear onset of catalytic activity above 320 °C was previously determined.[21,22] Above this temperature, at 350 °C (not shown in Table S4), a considerably higher conversion of CCl_2FCClF_2 was obtained for β-AlF_3 as for A1 or A3. In addition, surface area of β-AlF_3 (~30 $m^2\ g^{-1}$) is two or four times lower than that of A1 and A3. This indicates that, on the surface area basis, activity of the two aerogels is much lower than that of the reference β-AlF_3. On the other side, collapsed material, C1, with relatively low surface area of 29 $m^2\ g^{-1}$, shows very high catalytic activity that is comparable to that of the most active materials from the previous study. It should be also pointed out that some of the latter materials had surface areas that were almost ten times larger as that of C1 which additionally emphasizes the outstanding catalytic performance of this material. Striking difference in the catalytic activity between C1 on one side and the two aerogels, A1 and A3, on the other is rationalized in reference to the spectroscopic findings (see Figure 3 in the article). For all three materials (-C samples in Figure 3), disappearance of labile OH/H_2O species can be noticed and can be attributed to a combination of chemical and thermal effects. The latter being probably more important since it was found that similar removal of labile OH/H_2O can be accomplished by evacuation at 300 °C (cf. with -D samples in Figure 3). Chemical processes are probably less effective because of a lower overall reactivity of CCl_2FCClF_2, at least when A1 and A3 are concerned. Worth noting, bulk OH/H_2O species remain practically unchanged in all catalytic runs which is an additional indication that these species reside within the bulk of the primary particles and are not involved in surface processes.

As inferred from IR spectra, the only explicit difference between the catalytically inactive aerogels, A1 and A3, and the active C1 is the absence of MeO species in the latter. These species exhibit a remarkable thermal and chemical stability. Inactivity of both aerogels can therefore be ascribed to MeO species that presumably block the catalytically relevant strong Lewis acid sites and largely deactivate the surface. Deactivation is assumed to be achieved in two ways: (i) by direct bonding of MeO species to Lewis acid Al^{3+} sites, $Al^{\delta+}\cdots O^{\delta-}$–CH3, and (ii) by effective steric shielding that prevents further reactions on these sites, e.g. activation with bulkier CCl_2FCClF_2 molecules. Activation of AlF_3-based materials is commonly associated with the removal of surface OH/H_2O and other species that block the Lewis acid sites. This is usually achieved by mild fluorinating agents, among them CFCs, net effect is at least partial fluorination, i.e. replacement of surface Al–OH with Al–F.[6,21,25] In contrast to C1, removal of surface OH/H_2O species from A1 and A3 is apparently not sufficient to attain catalytic activity because of the incapacity of CCl_2FCClF_2 to remove the MeO groups that remain bonded to the strong Lewis sites. Efficient removal of

MeO species was achieved only by treatment with CCl_2F_2 (A3-F in Figure 3). Accordingly, the CCl_2F_2-treated A3-F became catalytically active (Table S4). This gives credibility to the above presumptions, *i.e.* removal of surface MeO species unblocks the strong Lewis acid sites that are thereafter accessible to CCl_2FCClF_2 and capable to catalyze its isomerization.

Table S4. Catalytic behaviour in isomerization of CCl_2FCClF_2 to CCl_3CF_3 compared to that of some previously investigated reference AlF_3-based catalysts[21]. Tests performed at 300 °C after activation at up to 350 °C.

Sample	Product distribution, relative yield (%)	
	CCl_2FCClF_2	CCl_3CF_3
A1	99.8	0.1
A3	97.8	0.3
A3-F	32.9	43.1
C1	3.6	70.6
β-AlF_3[a]	99.9	<0.1
F-γ-Al_2O_3[a]	11.9	57.9
ACF[a]	3.0	70.5
HS-AlF_3-FSG[a]	2.7	71.9
HS-AlF_3-OD[a]	2.8	71.7

[a]Data from[21]: fluorinated γ-alumina (F-γ-Al_2O_3), aluminium chlorofluoride (ACF), high surface area AlF_3 (HS-AlF_3) obtained by the fluoride sol-gel (-FSG) or oxidative decomposition (-OD) routes.

7) References

(1) Rüdiger, S.; Eltanany, G.; Groβ, U.; Kemnitz, E. *J. Sol-Gel Sci. Technol.* **2007**, *41*, 299–311.

(2) Kemnitz, E.; Groβ, U.; Rüdiger, S.; Shekar, C. S. *Angew. Chem. Int. Ed.* **2003**, *42*, 4251–4254.

(3) Skapin, T. *J. Mater. Chem.* **1995**, *5*, 1215–1222.

(4) Bozorgzadeh, H.; Kemnitz, E.; Nickkho-Amiry, M.; Skapin, T.; Winfield, J. M. *J. Fluorine Chem.* **2001,** *110*, 181–189.

(5) Dambournet, D.; Eltanamy, G.; Vimont, A.; Lavalley, J.-C.; Goupil, J.-M.; Demourgues, A.; Durand, E.; Majimel, J.; Rudiger, S.; Kemnitz, E.; Winfield, J. M.; Tressaud, A. *Chem. Eur. J.* **2008**, *14*, 6205–6212.

(6) Ruediger, S. K.; Groβ, U.; Feist, M.; Prescott, H. A.; Shekar, S. C.; Troyanov, S. I.; Kemnitz, E. *J. Mater. Chem.* **2005**, *15*, 588–597.

(7) Rüdiger, S.; Groβ, U.; Kemnitz, E. *J. Fluorine Chem.* **2007,** *128*, 353–368.

(8) Groβ, U.; Rüdiger, S.; Kemnitz, E.; Brzezinka, K.-W.; Mukhopadhyay, S.; Bailey, C.; Wander, A.; Harrison, N. *J. Phys. Chem. A* **2007**, *111*, 5813 –5819.

(9) Dambournet, D.; Demourgues, A.; Martineau, C.; Pechev, S.; Lhoste, J.; Majimel, J.; Vimont, A.; Lavalley, J.-C.; Legein, C.; Buzare, J.-Y.; Fayon, F.; Tressaud, A. *Chem. Mater.* **2008**, *20*, 1459–1469.

(10) Vimont, A.; Lavalley, J.-C.; Francke, L.; Demourgues, A.; Tressaud, A.; Daturi, M. *J. Phys. Chem. B* **2004**, *108*, 3246–3255.

(11) Scholz, G.; Brehme, S.; König, R.; Heidemann, D.; Kemnitz, E. *J. Phys. Chem. B* **2010**, *114*, 10535–10543.

(12) Dambournet, D.; Demourgues, A.; Martineau, C.; Durand, E.; Majimel, J.; Legein, C.; Buzare, J.-Y.; Fayon, F.; Vimont, A.; Leclerc, H.; Tressaud, A. *Chem. Mater.* **2008**, *20*, 7095–7106.

(13) Yang, Q.; Kong, M.; Fan, Z.; Meng, X.; Fei, J.; Xiao, F.-S. *Energy Fuels* **2012**, *26*, 4475–4480.

(14) Zaki, T. *J. Colloid Interface Sci.* **2005**, *284*, 606–613.

(15) Dambournet, D.; Demourgues, A.; Martineau, C.; Durand, E.; Majimel, J.; Vimont, A.; Leclerc, H.; Lavalley, J.-C.; Daturi, M.; Legein, C.; Buzare, J.-Y.; Fayon, F.; Tressaud, A. *J. Mater. Chem.* **2008**, *18*, 2483–2492.

(16) Francke, L.; Durand, E.; Demourgues, A.; Vimont, A.; Daturi, M.; Tressaud, A. *J. Mater. Chem.* **2003**, *13*, 2330–2340.

(17) Barclay, C. H.; Bozorgzadeh, H.; Kemnitz, E.; Nickkho-Amiry, M.; Ross, D. E. M.; Skapin, T.; Thomson, J.; Webb, G.; Winfield, J. M. *J. Chem. Soc., Dalton Trans.* **2002**, 40–47.

(18) Busca, G.; Rossi, P. F.; Lorenzelli, V.; Benaissa, M.; Travert, J.; Lavalley, J.-C. *J. Phys. Chem.* **1985**, *89*, 5433–5439.

(19) Boiadjiev, V.; Tysoe, W. T. *Chem. Mater.* **1998**, *10*, 334–344.

(20) Beebe, T. P. Jr.; Crowell, J. E.; Yates, J. T. Jr. *J. Phys. Chem.* **1988**, *92*, 1296–1301.

(21) Skapin, T.; Mazej, Z.; Makarowicz, A.; Jesih, A.; Nickkho-Amiry, M.; Schroeder, S. L. M.; Weiher, N.; Žemva, B.; Winfield, J. M. *J. Fluorine Chem.,* **2011**, *132*, 703–712.

(22) Bozorgzadeh, H.; Kemnitz, E.; Nickkho-Amiry, M.; Skapin, T.; Winfield, J. M. *J. Fluorine Chem.,* **2003**, *107*, 45–52.

(23) Murthy, J. K.; Gross, U.; Rüdiger, S.; Rao, V. V.; Kumar, V. V.; Wander, A.; Bailey, C. L.; Harrison, N. M.; Kemnitz, E. *J. Phys. Chem. B,* **2006**, *110*, 8314–8319.

(24) Bozorgzadeh, H.; Kemnitz, E.; Nickkho-Amiry, M.; Skapin, T.; Tate, G. D.; Winfield, J. M. *J. Fluorine Chem.,* **2001**, *112*, 225–232.

(25) Kemnitz, E.; Winfield, J. M. In *Advanced Inorganic Fluorides: Synthesis, Characterization and Application*; Nakajima, T.; Žemva, B.; Tressaud, A. Eds.; Elsevier Science S.A.: Laussane, 2000, Chapter 12, pp 367–401.